J. Phys. IV France **11** (2001)

Tow-dimensional simulation of a pulsed-power electronegative discharge

B. Ramamurthi and D.J. Economou

Plasma Processing Laboratory, Department of Chemical Engineering, University of Houston, Houston, TX 77204-4792, U.S.A.

Abstract. A two-dimensional self-consistent fluid model was developed to study the spatio-temporal dynamics of a pulsed power (square-wave modulated) inductively coupled electronegative (chlorine) discharge. The coupled equations for plasma power deposition, electron temperature, and charged and neutral species densities were solved simultaneously to capture the spatio-temporal evolution of the discharge. Simulation results showed separation of the plasma into an electronegative core and an electropositive edge during the active glow (power on) fraction of the cycle, and the formation of a positive ion/negative ion (ion-ion) plasma in the afterglow (power off) fraction of the cycle. During the early active glow, the negative ion flux is convection dominated near the quartz window under the planar coil of the ICP reactor. This is due to the emergence of relatively large electrostatic fields, leading to a self-sharpening negative ion front propagating into the plasma.

1 Introduction

Low pressure (1-100 mTorr) glow discharge plasmas are used extensively in microelectronics processing for etching and deposition of thin films [1]. Pulsed power operation (e.g., square-wave modulated power input to the plasma) can offer potential improvements to reactor performance. For example, etch or deposition rate and uniformity may be improved [2,3], particulate density can be reduced [4], and anomalous etch profiles may be suppressed [5].

Pulsed power electronegative discharges are of particular practical importance since the vast majority of gases used for plasma processing are electronegative. In such plasmas, negative ions replace electrons as the dominant negative-charge carrier sometime in the afterglow, provided the afterglow phase is long enough. A positive ion/negative ion (ion-ion) plasma is then formed and negative ions can escape the discharge [6]. Since the temperature and mass of negative ions are comparable to those of positive ions, the flux of positive and negative ions will be equally anisotropic, reducing differential charging on the walls of microscopic features on the wafer surface. Ahn et al. [5] applied a low frequency bias (600 kHz) in the afterglow of a pulsed chlorine discharge to achieve significant reduction in charging damage (notching) compared to a continuous wave (cw) plasma. This was attributed to alternate extraction [7] of positive ions and negative ions leading to reduced surface charging.

In order to improve our understanding of pulsed plasmas in electronegative gases, and elucidate how these plasmas may affect processing, it becomes necessary to model the spatio-temporal plasma evolution in realistic reactor geometries. Existing self-consistent pulsed plasma models and simulations are limited to well mixed (0-D) [8,9] and one-dimensional (1-D) works [6]. In this article, a two-dimensional (2-D) self-consistent fluid model is developed to simulate the spatio-temporal evolution of an inductively coupled pulsed chlorine discharge in a GEC Reference Cell [10]. In previous studies, a modular approach was used to simulate cw plasma operation [11], in which only the "steady state" was of interest. In contrast, in the present work, the coupled equations for plasma power deposition, electron

temperature, and charged and neutral species densities were *solved simultaneously* to capture the discharge evolution.

2 Model Formulation

Fig. 1 shows a schematic of the inductively coupled GEC Reference Cell, which can generate a high density plasma inside a chamber bounded by a quartz window and metal walls. The plasma is driven by a planar coil powered at 13.56 MHz. The RF current in the coil produces a time-varying magnetic field, which in turn induces an azimuthal electric field heating the plasma electrons. The fluid approximation was used since $\lambda/L \sim 0.1$, where λ is the species mean-free path (~ 0.5 cm at 10 mTorr) and L is a characteristic dimension of the reactor (~ 5 cm). The model (see Table below) consists of the electromagnetic equation for the self-consistent azimuthal electric field powering the plasma, an equation for the electron temperature (assuming Maxwellian electrons) and mass continuity equations for the charged (Cl^+, Cl_2^+ and Cl^-) and neutral (Cl) species. Details of the formulation may be found in published works [12,13]. The electron density is calculated by charge neutrality. This implies that the thin sheath near the reactor walls is not included in the simulation. Since the sheath is only 100s of microns thick in the high density plasma, boundary conditions are effectively applied at the geometric location of the walls. Due to azimuthal symmetry, only a 2-D section (r-z plane) of the reactor was simulated. The reaction set for chlorine was the same as before [13], except that the charge exchange reaction $Cl^+ + Cl_2 \rightarrow Cl + Cl_2^+$ [14] was also incorporated in the chemistry set. For typical flow rates used in the GEC cell (few 10s of sccm), the gas residence time is much longer than the species reaction time. Hence flow has little effect on species concentrations.

Table 1. The equation set used in the simulation

	Equation	Boundary conditions
Azimuthal Electric field:	$\frac{1}{r}\frac{\partial}{\partial r}\left(r\frac{\partial E_\theta}{\partial r}\right)+\frac{\partial^2 E_\theta}{\partial z^2}-\frac{E_\theta}{r^2}+\frac{\omega^2}{c^2}K_c E_\theta = -j\omega\mu_0 J_\theta^i$	$E_\theta = 0$
Ion Continuity:	$\frac{\partial n_i}{\partial t} = -\nabla\cdot\left(s_i\mu_i n_i\vec{E} - D_i\nabla n_i\right)+\sum_j R_{ji}$	$p \approx 0; n = 0$
Electron Temperature:	$\frac{\partial}{\partial t}\left(\frac{3}{2}n_e T_e\right) = -\nabla\cdot\left(-K\nabla T_e+\frac{5}{2}\vec{\Gamma}_e T_e\right)+P-\sum_j R_{je}\Delta H_j$	$\vec{q}_e = \frac{5}{2}\vec{\Gamma}_e T_e$
Neutral Transport:	$\frac{\partial n_{cl}}{\partial t} = -\nabla\cdot\left(-D_{cl}\nabla n_{cl}\right)+\sum_j R_{jcl}-\frac{n_{cl}}{\tau_{res}}$	$-D_{cl}\nabla n_{cl} = \frac{\gamma}{2(2-\gamma)}n_{cl}v_{cl}-\Gamma_{cl^+}$
Ambipolar Electric Field:	$\vec{E} = \frac{D_{p_1}\nabla p_1 + D_{p_2}\nabla p_2 - D_n\nabla n - D_e\nabla n_e}{\mu_{p_1}p_1+\mu_{p_2}p_2+\mu_n n+\mu_e n_e}$	

In the above equations, E_θ is the azimuthal electric field, ω is the driving RF frequency, K_c is the complex permittivity of the plasma (which depends on the electron density), J_θ^i is the impressed current density in the coil, s_i represents the number of elementary charges of the ion species, and μ and D are the species mobilities and diffusivities, respectively. E is the ambipolar electrostatic field (comprising of two components E_r and E_z), q_e is the electron energy flux, $Re(\sigma_p)$ is the real part of the complex plasma conductivity σ_p, n_e (=p_1+p_2−n) is the electron density, where, p_1 is the density of Cl^+, p_2 is the density of Cl_2^+, and n is the density of Cl^- (subscripts p_1, p_2 and n also denote the properties of these species, respectively). K_e is the thermal conductivity of the electron gas, Γ_e is the electron flux, γ is the surface recombination coefficient of Cl atoms on the wall (=0.1), v_{cl} is the thermal velocity of these atoms, and Γ_{cl}^+ is the flux of Cl^+ ions on the wall. Species mobilities and diffusivities were the same as before [13].

3 Method of Solutio

The equation for the azimuthal e
The rest of the partial differer
Galerkin (SUPG) method [15], t
is better able to catch sharp gra
were integrated in time using
obtained. The convergence crite
respect to the average i.e.,

$$\varepsilon_j = \frac{1}{V^{1/2}}$$

where ε_j, u_j, $\langle u_j\rangle$ are the toler
density), and solution variable
volume, and T_p is the pulse peri
condition was tested at the end
tolerance was satisfied. The cho
temperature and 1% for the rad
the longer time scale of neutral s

4 Results and Discus

The base case parameters used
deposited in the plasma, 10 kH
and a duty ratio of 0.5 (50% ful
case conditions and the periodic
to the power-on fraction of the
(50-100 μs).

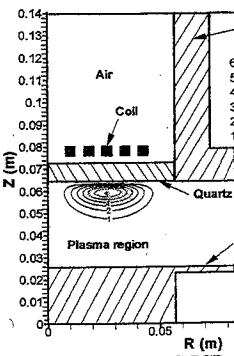

Figure 1. Schematic of the GEC-ICP
the quasi-steady power depo

Besides showing the re
the active glow. Power is dep
conditions is ~ 1 cm. The locali
electron temperature profile (n
whole plasma region between t

simultaneously to capture the

ence Cell, which can generate a
netal walls. The plasma is driven
oduces a time-varying magnetic
: plasma electrons. The fluid
ee path (~ 0.5 cm at 10 mTorr)
see Table below) consists of the
owering the plasma, an equation
ass continuity equations for the
lation may be found in published
This implies that the thin sheath
is only 100s of microns thick in
at the geometric location of the
the reactor was simulated. The
rge exchange reaction $Cl^+ + Cl_2$
l flow rates used in the GEC cell
es reaction time. Hence flow has

Boundary conditions
$E_\theta = 0$
$p \approx 0; n = 0$
$\bar{q}_e = \frac{5}{2}\bar{\Gamma}_e T_e$
$-D_{cl}\nabla n_{cl} = \frac{\gamma}{2(2-\gamma)} n_{cl} v_{cl} - \Gamma_{cl^+}$

driving RF frequency, K_c is the
nsity), J_θ^i is the impressed current
: ion species, and μ and D are the
:trostatic field (comprising of two
real part of the complex plasma
lensity of Cl^+, p_2 is the density of
: the properties of these species,
the electron flux, γ is the surface
rmal velocity of these atoms, and
es were the same as before [13].

3 Method of Solution

The equation for the azimuthal electric field E_θ was discretized using the Galerkin finite element method. The rest of the partial differential equations were discretized using the Streamline Upwind Petrov-Galerkin (SUPG) method [15], to yield a system of implicit ordinary differential equations (ODE). SUPG is better able to catch sharp gradients compared to the standard Galerkin method. The resulting ODEs were integrated in time using Backward Difference Formulae [16], until a periodic steady state was obtained. The convergence criterion was set by evaluating the L^2 norm of the solution normalized with respect to the average i.e.,

$$\varepsilon_j = \frac{1}{V^{1/2}}\left[\int_\Omega \left\{\left(\frac{u_j}{\langle u_j\rangle}\right)_{(i+1)T_p} - \left(\frac{u_j}{\langle u_j\rangle}\right)_{iT_p}\right\}^2 d\Omega\right]^{1/2} \qquad (1)$$

where ε_j, u_j, $\langle u_j\rangle$ are the tolerance parameter, solution variable (e.g., electron temperature, species density), and solution variable averaged over the domain Ω of interest, respectively. V is the plasma volume, and T_p is the pulse period of the square-wave power-modulation cycle. The above convergence condition was tested at the end of each pulse, and integration was terminated when the user-specified tolerance was satisfied. The chosen tolerances were 0.5% for the charged species, 0.01% for the electron temperature and 1% for the radical density. The radical density was the slowest to converge because of the longer time scale of neutral species chemistry and transport.

4 Results and Discussion

The base case parameters used in the simulation were 20 mTorr pressure, 320 W peak input power deposited in the plasma, 10 kHz pulsing frequency (100 microseconds pulse period) of the square wave, and a duty ratio of 0.5 (50% full power-on, 50% all power off). All results shown below are for the base case conditions and the periodic steady-state achieved after a number of cycles. Also, *active glow* refers to the power-on fraction of the cycle (0-50 μs), and *afterglow* refers to the power-off fraction of the cycle (50-100 μs).

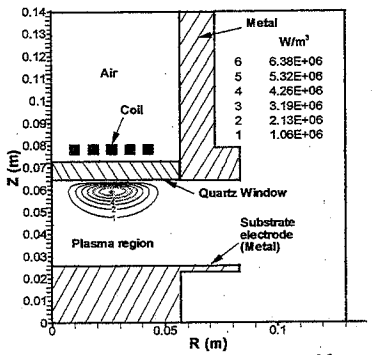

Figure 1. Schematic of the GEC-ICP reactor with the quasi-steady power deposition profile

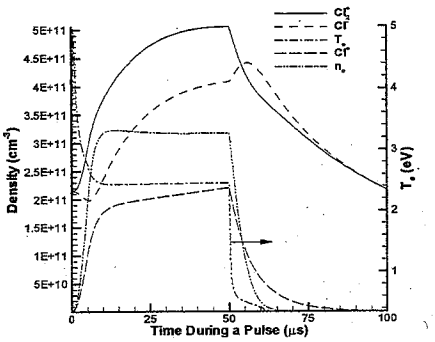

Figure 2. Species density and electron temperature evolution (right axis) at the reactor center

Besides showing the reactor geometry, Figure 1 also shows the power deposition profile late in the active glow. Power is deposited underneath and near the planar coil. The skin depth under these conditions is ~ 1 cm. The localized power deposition profile results in a rather localized maximum of the electron temperature profile (not shown). Although the electron temperature is highest near the coils, the whole plasma region between the quartz window and the substrate electrode is kept warm due to the high

thermal conductivity of the electron gas in the high density plasma (electron thermal conductivity is proportional to electron density).

The evolution of electron temperature and species densities at the *reactor center* is shown in Fig. 2. These results have been observed experimentally [5,17,18]. The electron temperature is determined by the balance (or lack thereof during transients) between ionization (atomic and molecular chlorine), attachment to molecular chlorine, and ambipolar diffusion losses to the walls. Since the electron density is very low at the start of a pulse, the electron temperature attains a relatively high value initially (> 5 eV), dropping to a quasi-steady value ~ 10 μs into the active glow. At this time ionization is balanced by attachment and ambipolar diffusion losses to the walls. The initial rapid decrease in electron temperature when power is turned off is due to electron losses in high threshold energy processes. The density of both positive ions increases monotonically during the active glow as production by ionization exceeds ion losses. In the afterglow, however, ionization is quenched (T_e plummets) and the positive ion density decreases with time. The Cl^+ density is lower when compared to Cl_2^+ density in part due to the charge exchange reaction converting Cl^+ to Cl_2^+. This reaction causes the Cl^+ density to decay to very low values late in the afterglow. The electron density increases monotonically during the active glow, and then drops monotonically during the afterglow. About 15 μs into the afterglow, the electron density has reached a very low value. This is when a positive ion/negative ion (ion-ion) plasma forms. The negative ion is Cl^- and the positive ion is predicted to be mainly Cl_2^+ as also found experimentally [7]. Transport processes play a role in the time

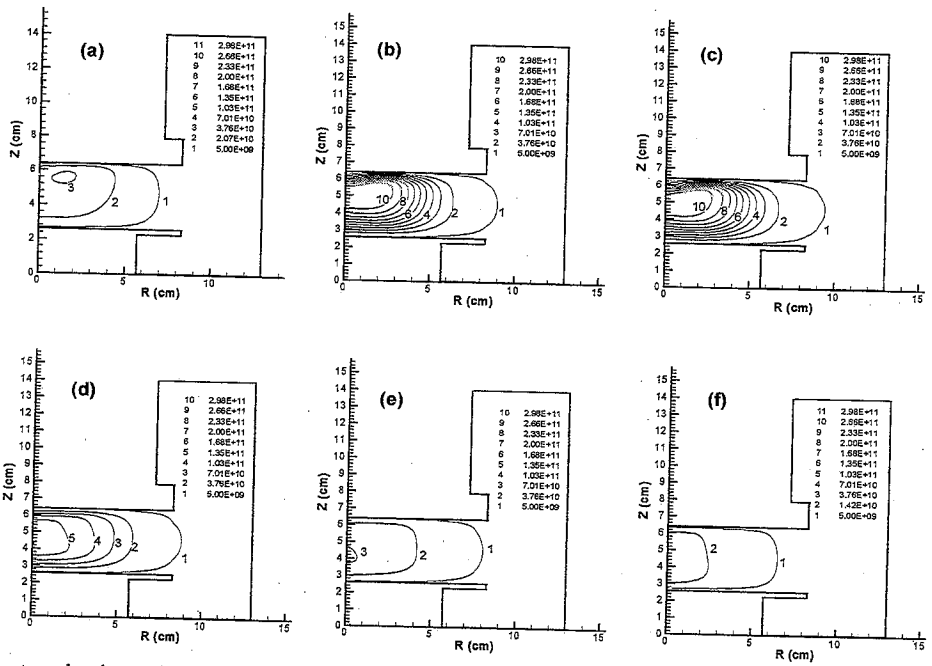

Figure 3. Electron density evolution for times a) 2 b) 10 c) 50 d) 53 e)56 and f) 60 μs during a pulse. Density is in cm^{-3}.

evolution of the negative ion density [19]. Squeezing of the negative ion density profiles towards the plasma center by the emerging electrostatic fields (see also Fig. 5 below) is a major contributor to the increase in negative ion density at the reactor center during the active glow. Also, the decay of the negative ion density in the afterglow is mainly due to back diffusion of the negative ions towards the reactor walls as the electrostatic fields disintegrate.

The spatiotemporal evo
Fig. 3, for 2, 10, 50, 53, 56 and
the electron temperature (Fig.
density increases with time. Th
also peaks. In addition, the ele
larger concentration of nega
electronegativity, the electron
electropositive plasmas), leadin

About 10 μs into the a
state and changes very little up
between electron production (
and ambipolar diffusion losses
two parts: an electronegative
(compare Fig. 3c to Fig. 4d), an

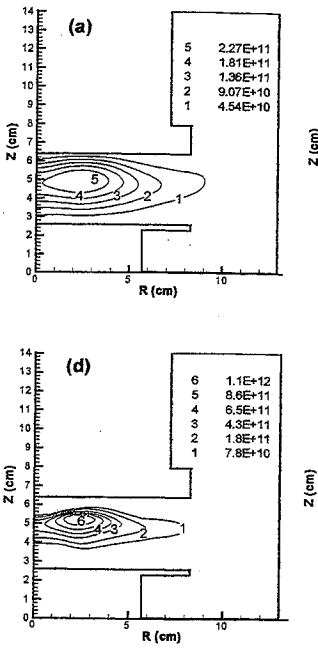

Figure 4. Cl^- density evolution for time

density is very low. For the same
compared to the edge. Once p
quenched since the electron temp
are lost by attachment and diffu
electrons keep disappearing, the
the plasma by the electrostatic
diffusion), and the electron dens
into the afterglow; the plasma at

The Cl^- density profile ev
ion are present close to the axial

electron thermal conductivity is

reactor center is shown in Fig.
on temperature is determined by
tomic and molecular chlorine),
walls. Since the electron density
latively high value initially (> 5
is time ionization is balanced by
decrease in electron temperature
y processes. The density of both
ction by ionization exceeds ion
s) and the positive ion density
ensity in part due to the charge
sity to decay to very low values
the active glow, and then drops
electron density has reached a
a forms. The negative ion is Cl^-
entally [7]. Transport processes

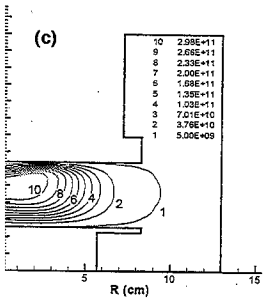

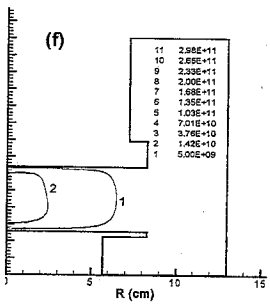

ing a pulse. Density is in cm^{-3}.

n density profiles towards the
) is a major contributor to the
glow. Also, the decay of the
the negative ions towards the

The spatiotemporal evolution of electron density (cm^{-3}) for the base case conditions is shown in Fig. 3, for 2, 10, 50, 53, 56 and 60 µs. Early in the active glow (Fig. 3a), the electron density is low, and the electron temperature (Fig. 2) is high, causing ionization to exceed electron losses. Thus the electron density increases with time. The peak electron density is directly under the coils where power deposition also peaks. In addition, the electron density gradients are rather weak, due to the existence of a much larger concentration of negative ions (10x higher, see Fig. 4a). In regions of high plasma electronegativity, the electron diffusivity is enhanced (over and above the ambipolar diffusivity of electropositive plasmas), leading to smoother density gradients.

About 10 µs into the active glow (Fig. 3b), the electron density profile reaches a quasi steady-state and changes very little up to the end of the active glow (Fig. 3c). At this stage, there is a balance between electron production (atomic and molecular ionization) and destruction processes (attachment and ambipolar diffusion losses to the walls). Also, during this time period the plasma zone is separated in two parts: an electronegative core where the negative ion density dominates the electron density (compare Fig. 3c to Fig. 4d), and an electropositive edge surrounding the core where the negative ion

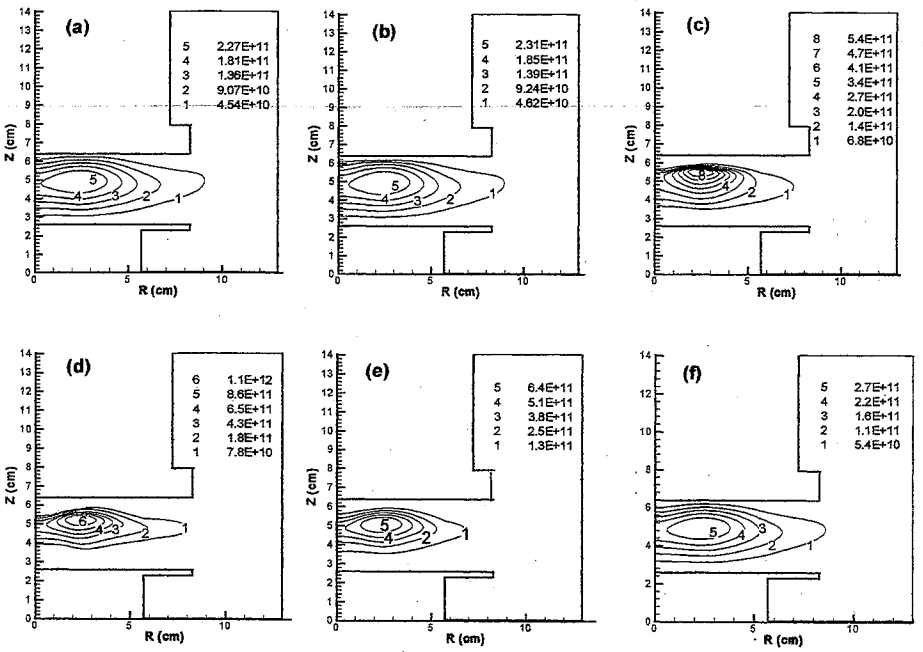

Figure 4. Cl^- density evolution for times a) 0, b) 1, c) 5, d) 50, e) 60 and f) 90 µs. Density is in cm^{-3}.

density is very low. For the same reason as above, the electron density gradients are smoother in the core compared to the edge. Once power is turned off, high threshold processes, such as ionization, are quenched since the electron temperature decays very rapidly (within a few µs) in the afterglow. Electrons are lost by attachment and diffusion to the walls leading to a fast decrease in the electron density. As electrons keep disappearing, the plasma electronegativity keeps increasing (negative ions are trapped in the plasma by the electrostatic fields), the electron diffusivity keeps increasing (to the point of *free* diffusion), and the electron density gradients keep decreasing. Most of the electrons are lost by ~ 15 µs into the afterglow; the plasma at this stage turns into an ion-ion plasma.

The Cl^- density profile evolution is shown in Figs. 4a-4f. At the start of a pulse (Fig. 4a), negative ion are present close to the axial walls due to diffusion in the ion-ion plasma formed in the late afterglow

of the previous pulse. As the electron temperature starts to increase, the ambipolar electric field also increases, causing negative ions to be convectively squeezed towards the plasma center. This squeezing of negative ions is stronger near the quartz window under the coils since the electron temperature is higher in that region. In fact the negative ion front is self sharpening [19]. The negative ion density profile evolves throughout the active glow. Since there is negligible flux of negative ions to the wall during the active glow, the quasi-steady state profile of negative ions shown in Fig. 4d is the result of an approximate balance between production by attachment and destruction by detachment and ion-ion recombination.

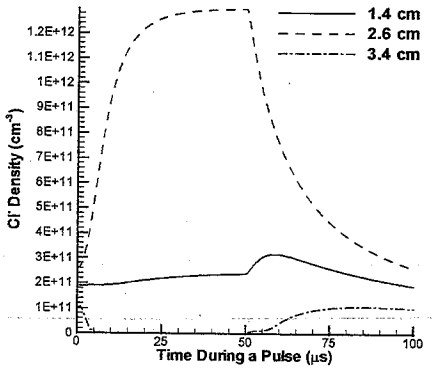

Figure 5. Negative ion density evolution at a radius of 2.4 cm for three axial locations

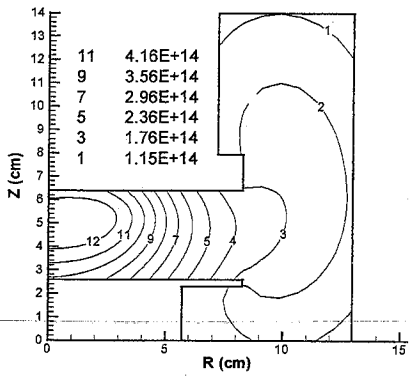

Figure 6. Two dimensional quasi steady-state Cl atom density (cm^{-3}) profile

The time evolution of the negative ion density depends on the spatial position at which the negative ions are monitored, as illustrated in Fig. 5. Here the negative ion density evolution is shown at three axial locations (1.4 cm, 2.6 cm, and 3.4 cm from the substrate electrode, points 1, 2, and 3, respectively) all at a fixed radius of 2.4 cm. At point 3 (closest to the quartz window), there is an initial abrupt drop in the negative ion density as negative ions are squeezed out of the edge (and into the plasma core) due to the emergence of the ambipolar field, as power is turned on. The field exists throughout the active glow, keeping the negative ion density very low in that region. In the afterglow, the field disintegrates quickly allowing negative ions to escape back to the wall, thereby leading to a rise in the negative ion density at point 3. A similar situation exists near the substrate electrode (point 1). However, the ambipolar field is not strong enough at that location (due to the lower electron temperature) to keep negative ions completely out. At the center of the discharge (point 2), the negative ion density increases monotonically during the active glow as negative ions pile up (due to the squeezing referred to above) near the center. In the afterglow, the negative ion density decreases monotonically due to negative ions diffusing back towards the walls.

Fig. 6 shows the quasi steady-state profile of the Cl atom density. The Cl atom density depends mainly on the electron density and the wall recombination probability of Cl atoms. Since the neutral response time scale is much longer than the pulse period, the neutral density profiles are modulated only weakly. In fact, the neutral density responds to the average power (average electron density), whereas the charged species densities respond to the power modulation (Fig. 2). A peak in Cl atom density occurs in the core region of the discharge where the electron density also peaks. The Cl atom density in the outer region is low due to wall recombination and negligible production of Cl atoms in that region.

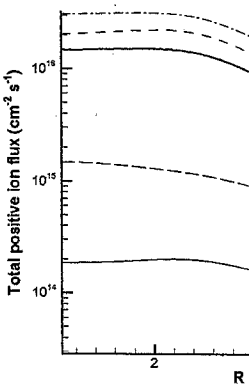

Figure 7. Total positive ion flux evolut

Etch rate depends on th
depends on the ion flux profile
of the positive ion flux profile,
the early active glow (0-5 μs)
afterglow and the time-average
plasma is well confined in the ra

5 Conclusions

A two-dimensional self-consist
(chlorine) plasma was develope
deposition profiles, electron ter
element method to capture the s
on) fraction of the cycle, spor
electropositive edge was obser
glow due to the emerging ambip
near the quartz window under th
of the negative ion density prof
the reactor. The electron densit
the afterglow, leaving behind a
free diffusion and ion-ion recom
and lowest in the chamber surr
electrode radius were very non
absence of capacitively coupled

References

[1] M. A. Lieberman and A. J. I
(J. Wiley & Sons, New York, 1
[2] R. Boswell and R. Porteous,
[3] P. Jiang, D. J. Economou, ar
D. J. Economou, J. Electrochem
[4] J. Verdeyen, J. Bederman, a
[5] T. H. Ahn, K. Nakamura and

he ambipolar electric field also
e plasma center. This squeezing
ince the electron temperature is
[19]. The negative ion density
lux of negative ions to the wall
own in Fig. 4d is the result of an
ion by detachment and ion-ion

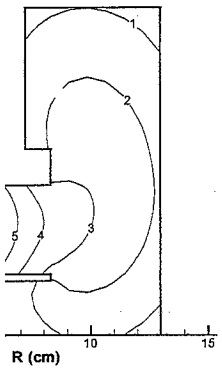

ıal quasi steady-state
y (cm^{-3}) profile

ıe spatial position at which the
ɔn density evolution is shown at
e electrode, points 1, 2, and 3,
ıartz window), there is an initial
of the edge (and into the plasma
ı. The field exists throughout the
ɔn. In the afterglow, the field
thereby leading to a rise in the
te electrode (point 1). However,
er electron temperature) to keep
ıe negative ion density increases
he squeezing referred to above)
notonically due to negative ions

y. The Cl atom density depends
of Cl atoms. Since the neutral
ısity profiles are modulated only
ge electron density), whereas the
eak in Cl atom density occurs in
The Cl atom density in the outer
ıtoms in that region.

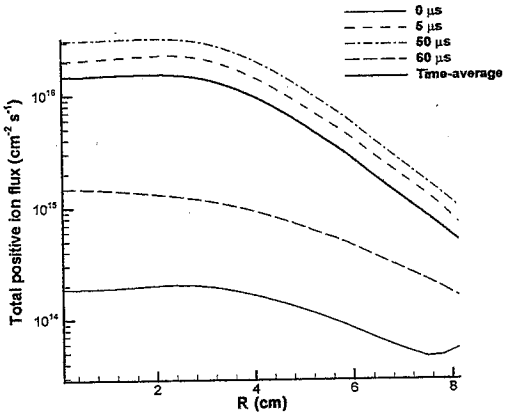

Figure 7. Total positive ion flux evolution on the substrate electrode during a pulse

Etch rate depends on the magnitude of the ion flux incident on a wafer and etch uniformity depends on the ion flux profile across the wafer radius. Hence it is worthwhile to examine the evolution of the positive ion flux profile, as shown in Fig. 7. The time-averaged flux over a cycle is also shown. In the early active glow (0-5 μs) the positive ion flux is low, albeit more uniform. The flux later in the afterglow and the time-average flux are very non-uniform. This is because the inductively coupled plasma is well confined in the radial direction in the absence of capacitive fields.

5 Conclusions

A two-dimensional self-consistent simulation of an inductively coupled pulsed-power electronegative (chlorine) plasma was developed based on the fluid approximation. The coupled equations for the power deposition profiles, electron temperature and species densities were solved simultaneously by a finite element method to capture the spatiotemporal evolution of the discharge. During the active glow (power on) fraction of the cycle, spontaneous separation of the plasma into an electronegative core and an electropositive edge was observed. Negative ions squeezed towards the plasma core during the active glow due to the emerging ambipolar electrostatic fields at the edge. This squeezing was more pronounced near the quartz window under the coil where power deposition takes place. As a result the time evolution of the negative ion density profiles showed completely opposite trends depending on spatial location in the reactor. The electron density decayed to very low values ~ 15 μs (for the conditions examined) into the afterglow, leaving behind a positive ion/negative ion (ion-ion) plasma which decayed by (almost) free diffusion and ion-ion recombination. The Cl atom density was found to be highest in the plasma core and lowest in the chamber surrounding the plasma zone. The positive ion profiles across the substrate electrode radius were very non-uniform suggesting a well confined inductively coupled plasma in the absence of capacitively coupled fields.

References

[1] M. A. Lieberman and A. J. Lichtenberg, Principles of Plasma Discharges and Materials Processing (J. Wiley & Sons, New York, 1994)
[2] R. Boswell and R. Porteous, J. Appl. Phys., 62, 3123 (1987)
[3] P. Jiang, D. J. Economou, and C. B. Shin, Plasma Chem Plasma Proc., 15, 383 (1995); S.-K. Park and D. J. Economou, J. Electrochem. Soc., 138, 1499 (1991)
[4] J. Verdeyen, J. Bederman, and L. Overzet, J. Vac. Sci. Technol. A, 8, 1851 (1990)
[5] T. H. Ahn, K. Nakamura and H. Sugai, Plasma Sources Sci. Technol. 5, 139 (1996)

[6] V. Midha and D. J. Economou, Plasma Sources Sci. Technol. 9, 256 (2000); R. N. Franklin and J. Snell, J. Phys. D: Appl. Phys., 32, 2190 (1999)
[7] S. Kanakasabapathy, L. Overzet, V. Midha and D. J. Economou, Appl. Phys. Lett., 78, 22 (2001)
[8] M. Meyyappan, J. Vac. Sci. Technol. A 14, 2122 (1996)
[9] S. Ashida and M. A. Lieberman, Jpn. J. Appl. Phys. 36, 854 (1997)
[10] P. J. Hargis et al., Rev. Sci. Instr. 65, 140 (1994)
[11] D. J. Economou, J. Feldsien, and R. S. Wise, in Electron Kinetics and Applications of Glow Discharges, edited by U. Kortshagen and L. D. Tsendin, NATO Advanced Research Workshop, Plenum (1998); R. Wise, D. Lymberopoulos and D. J. Economou, Appl. Phys. Lett., 68, 2499 (1996)
[12] D. P. Lymberopoulos and D. J. Economou, J. Res. Natl. Inst. Stand. Technol. 100, 473 (1995)
[13] D. P. Lymberopoulos and D. J. Economou, IEEE Trans. Plasma Sci. 23, 573 (1995)
[14] J. Helmsen, D. Hammer, J. Yamartino, P. Loewenhardt, IEEE Trans. Plasma Sci. 27, 58 (1999)
[15] A. N. Brooks and T. J. R. Hughes, Comp. Meth. in Appl. Mech. and Engr. 32, 199 (1982)
[16] G. D. Byrne and A. C. Hindmarsh, J. Comp. Phys. 70, 1 (1987)
[17] M. V. Malyshev, V. M. Donnelly, J. I. Colonell, S. Samukawa, J. Appl. Phys. 86, 4813 (1999)
[18] G. A. Hebner and C. B. Fledderman, J. Appl. Phys., 82, 2814 (1997)
[19] D. Kaganovich, D. J. Economou, B. N. Ramamurthi, and V. Midha, Phys. Rev. Lett., 84, 1918 (2000)

J. Phys. IV France **11** (2001)

Heat and mass tran
LPCVD process

V.G. Minkina

Heat & Mass Transfer Institu
Belarus

Thermodiffusion is shown
the silicon deposition rate
reactor the kinetic reactio
kinetic reaction have a pr
permit calculating the proc

1. INTRODUCTION

Chemical vapor deposition at lo
of semiconducting devices and
effect of pressure in the reacto
silicon layers. However, in son
kinetic deposition model. In the
taken that often disregard che
equipment and the quality of pr
chambers. In this work a series
regarding the variability the va
heterogeneous reactions that tak

2. THE MATHEMATICAL M

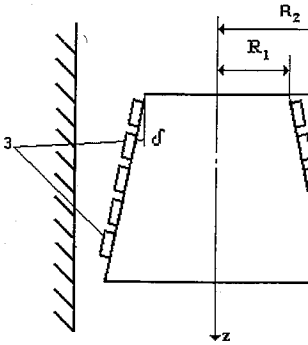

Figure 1. Scheme of the reactor: 1 - reac
2 - substrate holder, 3 - substrates.